

# Four-Point Planar Homography Algorithm for Rectification Photogrammetry: Development and Applications

2013-01-0780  
Published  
04/08/2013

Chad Hovey  
Hovey Consulting LLC

Angelo Toglia  
Collision Research & Analysis Inc

Copyright © 2013 SAE International  
doi:[10.4271/2013-01-0780](https://doi.org/10.4271/2013-01-0780)

## ABSTRACT

Photogrammetric techniques of analyzing vehicles and scenes for accident reconstruction are well documented and have appeared in various forms and levels of complexity over the years. Plane-to-plane rectification algorithms, frequently used for accident reconstruction, are subsets of a growing field of computer vision algorithms, which are rigorously developed in [1,2,3,4]. While these algorithms are well formulated, they are not well illustrated. It is often not clear how to leverage advancements in computer vision algorithms for the purposes of rectification photogrammetry in the context of accident reconstruction.

Perhaps as expected, a second strategy exists in the literature, which describes the use, as opposed to the development, of commercial computer programs for rectification photogrammetry [5,6,7,8]. Commercial software applications provide a robust and wide array of photogrammetric analysis. However, their use does not promote learning or insight into the mathematics of rectification algorithms, as the commercial program is compiled and guarded by the company as its intellectual property.

There is a gap between these two bodies of work. That gap is the elucidation of the mathematics and the algorithm used to connect planar homography mathematics with concrete examples and published results that can be used by analysts to validate their own algorithm implementation.

This paper helps bridge that gap. We first develop, in a simple yet robust way, the mathematical underpinning of the

four-point planar algorithm. Next, we state the algorithm, along with the underlying assumptions and requirements. Finally, we review and provide results from two case studies and a laboratory study, which can be used to validate subsequent implementations by other analysts. Novel to this work is the application of suitable pre-conditioned homography matrices to enable image rectification via direct solution using only four control points.

## INTRODUCTION

In the field of accident reconstruction, the spatial description of a body or mark that is captured in a photograph taken at the time of the accident but is no longer present at time of analysis is often of interest. For example, a tire skid mark, which may appear in an at-scene police photograph, may be absent at time of the analyst's scene inspection. The analyst may wish to include the position and length of the tire mark on an accident reconstruction diagram, in a robust and reliable way. To accomplish this, a process of rectification photogrammetry may be undertaken. This process seeks to map the geometry of interest from the photograph to the diagram.

The geometry, as it appears in the photograph, is naturally a perspective geometry. An object of a fixed size will appear larger in the foreground and smaller in the background. The size of the object will diminish to zero as its distance from the camera reaches infinity.

In contrast, the geometry as it appears in the reconstruction diagram is typically an orthographic plan view. Orthographic

geometry does not have the foreshortening attributes of perspective geometry. An orthographic projection can be considered a special case of a perspective projection, where the imaging focal length approaches infinity [1]. A camera with a telephoto lens illustrates this principle. For short focal lengths, a strong perspective geometry is apparent, and in extreme cases, a “fish-eye” effect will occur. For long focal lengths, perspectives are attenuated, and the image appears flattened, and in extreme cases, isometric. This principle may also be shown mathematically. Faugeras [9] demonstrated how an affine representation is embedded as a special case of a projective representation. The hierarchy of plane geometry is well described in Szeliski [3] and Quan [4].

The mathematics of perspective image-to-image mapping can be used to construct this map between two points-of-view [10]. Epipolar geometry describes the relationship between two perspective views of a three-dimensional object [2]. The mathematics produces what is known as the epipolar constraint, which gives rise to several object reconstruction algorithms. The eight-point algorithm for objects in three dimensions reduces to a four-point algorithm for cases when the object feature points are on a single planar surface [2].

Since this paper deals with planar homography, the minimum number of points required for the algorithm presented here is four. However, more than four points may be used in conjunction with a least-squares algorithm [1, 2, 11]. Use of more than four points can help reduce errors engendered by picking points. If four points alone produce errors, the analyst is encouraged to revisit the picked points to verify the accuracy of the point selection, or to consider the use of more than four points. Only the four-point approach is considered here since we have found this approach to perform well, absent of any negative side effects brought on by its simplicity.

## METHODS

### Geometry

Let body  $\Omega \subset \mathbb{R}^3$  have a planar surface  $\partial\Omega \subset \mathbb{R}^2$ . Let image plane  $\mathcal{A} \subset \mathbb{R}^2$  be spanned by the basis vectors  $[\hat{\mathbf{a}}_1, \hat{\mathbf{a}}_2]$  and be perpendicular to basis vector  $\hat{\mathbf{a}}_3$ . Let image plane  $\mathcal{B} \subset \mathbb{R}^2$  be spanned by the basis vectors  $[\hat{\mathbf{b}}_1, \hat{\mathbf{b}}_2]$  and be perpendicular to basis vector  $\hat{\mathbf{b}}_3$ . Note that our placement of planar basis vectors parallel to the image planes is general. Figure 1 illustrates the planes and bases.

Let point  $A$  be the focal point for image plane  $\mathcal{A}$  and the origin for the  $[\hat{\mathbf{a}}_1, \hat{\mathbf{a}}_2, \hat{\mathbf{a}}_3]$  basis vectors. The projection of point  $P \in \partial\Omega$  is located in the image plane  $\mathcal{A}$  by vector  $\tilde{x}$ , measured from origin  $A$ .

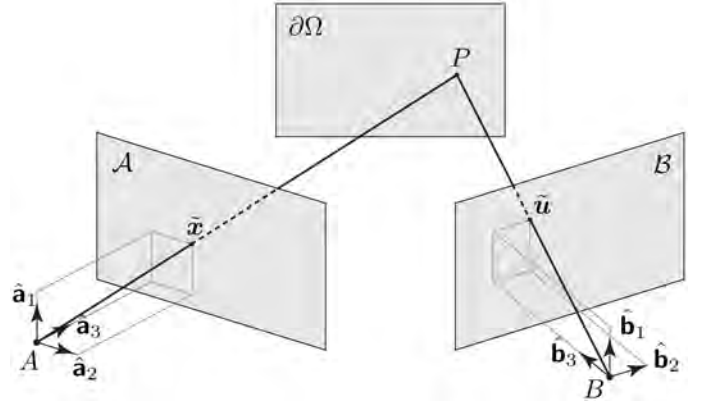


**Figure 1.** Relationship between a particle  $P$  on planar surface  $\partial\Omega$  of body  $\Omega$ , with projections onto  $\mathcal{A}$  and  $\mathcal{B}$  at  $\tilde{x}$  and  $\tilde{u}$ , respectively.

Similarly, let point  $B$  be the focal point for image plane  $\mathcal{B}$  and the origin for the  $[\hat{\mathbf{b}}_1, \hat{\mathbf{b}}_2, \hat{\mathbf{b}}_3]$  basis vectors. The projection of point  $P \in \partial\Omega$  is located in the image plane  $\mathcal{B}$  by vector  $\tilde{u}$ , measured from origin  $B$ . All basis vectors are dextral, orthonormal, ordered triads.

Let  $\Pi$  be the projection matrix that maps a vector in  $\mathbb{R}^3$  to an image plane in  $\mathbb{R}^2$ . The projection matrix is given by

$$\Pi = \begin{bmatrix} 1 & 0 & 0 \\ 0 & 1 & 0 \end{bmatrix}, \quad (1)$$

where the basis is assumed to be the same as the basis of the vector on which it operates. Then, the projection of  $\tilde{x}$  in the image plane  $\mathcal{A}$  is given by

$$\Pi \tilde{x} = x \hat{\mathbf{a}}_1 + y \hat{\mathbf{a}}_2. \quad (2)$$

Likewise, the projection of  $\tilde{u}$  in the image plane  $\mathcal{B}$  is given by

$$\Pi \tilde{u} = u \hat{\mathbf{b}}_1 + v \hat{\mathbf{b}}_2. \quad (3)$$

For any point located by  $\tilde{x}$ , we create a homogeneous vector  $x$  such that for  $\gamma \in \mathbb{R}$ ,  $\gamma \neq 0$ ,

$$x = \langle \gamma x, \gamma y, \gamma \rangle^T. \quad (4)$$

Similarly, for any point located by  $\tilde{u}$ , we create a homogeneous vector  $u$  such that for  $\lambda \in \mathbb{R}$ ,  $\lambda \neq 0$ ,

$$u = \langle \lambda u, \lambda v, \lambda \rangle^T. \quad (5)$$

When there is no possibility of confusion, we will use  $x$  interchangeably with  $\tilde{x}$ ; similarly  $u$  with  $\tilde{u}$ . See Ma [2], Szeliski [3], or Quan [4] for an explanation of the use of homogenous coordinates.

## Linear Map

Writing  $x$  and  $u$  as homogenous coordinates allows a linear relationship between these two vectors to be written,

$$u = Mx, \quad (6)$$

where  $M$  is a matrix that maps vector  $x$  to vector  $u$  [3]. Explicitly, this relationship takes the form

$$\begin{Bmatrix} \lambda u \\ \lambda v \\ \lambda \end{Bmatrix} = \begin{bmatrix} m_{11} & m_{12} & m_{13} \\ m_{21} & m_{22} & m_{23} \\ m_{31} & m_{32} & m_{33} \end{bmatrix} \begin{Bmatrix} \gamma x \\ \gamma y \\ \gamma \end{Bmatrix}_{\hat{\mathbf{a}}} \quad (7)$$

Using the third row of Eq. (7), and solving for  $\lambda$  gives

$$\lambda = \gamma(m_{31}x + m_{32}y + m_{33}). \quad (8)$$

Similarly, using Eq. (7) and solving for  $u$  and  $v$  by eliminating  $\lambda$  gives

$$u = \frac{m_{11}x + m_{12}y + m_{13}}{m_{31}x + m_{32}y + m_{33}}, \quad (9)$$

and,

$$v = \frac{m_{21}x + m_{22}y + m_{23}}{m_{31}x + m_{32}y + m_{33}}. \quad (10)$$

Since  $\gamma$  and  $\lambda$  are non-zero scaling constants, inspection of Eq. (8) reveals we can set  $m_{33} = 1$  without loss of generality. Consequently, there are eight unknowns,  $m_{11} \dots m_{32}$ , in  $M$ . To create eight equations that relate points  $x$  and  $u$ , we can select four separate points on planar surface  $\partial\Omega$ , as they appear in  $\mathcal{A}$  described with  $\langle x, y \rangle^T$  coordinates, and as they appear in  $\mathcal{B}$  described with  $\langle u, v \rangle^T$  coordinates.

## Four Control Points

Let four unique points on  $\partial\Omega$  have projections in  $\mathcal{A}$  described as

$$\mathbf{x}_k \quad k = 1, 2, 3, 4. \quad (11)$$

The same aforementioned points have projections in  $\mathcal{B}$  described as

$$\mathbf{u}_k \quad k = 1, 2, 3, 4. \quad (12)$$

No three points in either plane may be collinear. From Eqs. (9)-(10), we have

$$u_k = \frac{m_{11}x_k + m_{12}y_k + m_{13}}{m_{31}x_k + m_{32}y_k + 1}, \quad (13)$$

and

$$v_k = \frac{m_{21}x_k + m_{22}y_k + m_{23}}{m_{31}x_k + m_{32}y_k + 1}. \quad (14)$$

Rearranging each of the foregoing equations gives

$$u_k = m_{11}x_k + m_{12}y_k + m_{13} - m_{31}x_k u_k - m_{32}y_k u_k, \quad (15)$$

and

$$v_k = m_{21}x_k + m_{22}y_k + m_{23} - m_{31}x_k v_k - m_{32}y_k v_k. \quad (16)$$

Writing the components of  $m_{ij}$  in a  $(8 \times 1)$  column vector

$$\mathbf{m} = \langle m_{11}, m_{12}, m_{13}, m_{21}, m_{22}, m_{23}, m_{31}, m_{32} \rangle^T, \quad (17)$$

and writing out an explicit matrix form with  $k = 1, 2, 3, 4$  gives

$$\mathbf{Km} = \mathbf{b}, \quad (18)$$

where the  $(8 \times 8)$  matrix

$$\mathbf{K} = \begin{bmatrix} x_1 & y_1 & 1 & 0 & 0 & 0 & -x_1u_1 & -y_1u_1 \\ x_2 & y_2 & 1 & 0 & 0 & 0 & -x_2u_2 & -y_2u_2 \\ x_3 & y_3 & 1 & 0 & 0 & 0 & -x_3u_3 & -y_3u_3 \\ x_4 & y_4 & 1 & 0 & 0 & 0 & -x_4u_4 & -y_4u_4 \\ 0 & 0 & 0 & x_1 & y_1 & 1 & -x_1v_1 & -y_1v_1 \\ 0 & 0 & 0 & x_2 & y_2 & 1 & -x_2v_2 & -y_2v_2 \\ 0 & 0 & 0 & x_3 & y_3 & 1 & -x_3v_3 & -y_3v_3 \\ 0 & 0 & 0 & x_4 & y_4 & 1 & -x_4v_4 & -y_4v_4 \end{bmatrix}, \quad (19)$$

and the  $(8 \times 1)$  vector

$$\mathbf{b} = \begin{Bmatrix} u_1 \\ u_2 \\ u_3 \\ u_4 \\ v_1 \\ v_2 \\ v_3 \\ v_4 \end{Bmatrix}. \quad (20)$$

The explicit form  $K$  given in Eq. (19) may be verified with developments in Heckbert [12]. Inspection of  $K$  reveals its dependence on coordinates  $x$ ,  $y$ ,  $u$ , and  $v$ . In implementation,

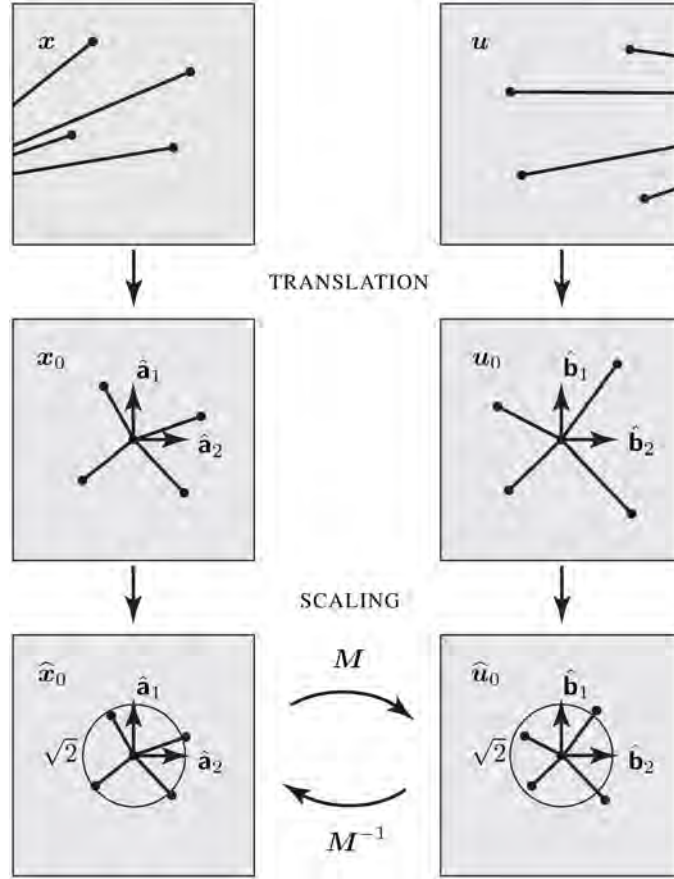


**Figure 2.** Concept of conditioning  $x$  and  $u$  prior to their use in Eq. (18). Note that we have oriented the axes to harmonize with the presentation in Figure 1.

these coordinates can be large numbers, typically with units of feet, meters, or pixels. Large numbers can cause  $K$  to be ill-conditioned. Furthermore, the units lead  $K$  to have elements tied to a measurement system. To eliminate both of these disadvantages, prior to forming the linear system in Eq. (18), we first condition the inputs  $x$ ,  $y$ ,  $u$  and  $v$ , similar to the strategy advocated by Hartley [11].

## Conditioning

Prior to their use in Eq. (18),  $x_k$  and  $u_k$  are translated so that the centroid of all control points is at the origin. This step, referred to as TRANSLATION in Figure 2, is defined by

$$(x_0)_k = \begin{Bmatrix} x_0 \\ y_0 \end{Bmatrix}_k = \begin{Bmatrix} x_k - \bar{x} \\ y_k - \bar{y} \end{Bmatrix}, \quad (21)$$

where

$$\bar{x} = \frac{1}{4} \sum_{k=1}^4 \tilde{x}_k \cdot \hat{\mathbf{a}}_1, \quad \bar{y} = \frac{1}{4} \sum_{k=1}^4 \tilde{x}_k \cdot \hat{\mathbf{a}}_2, \quad (22)$$

and

$$(u_0)_k = \begin{Bmatrix} u_0 \\ v_0 \end{Bmatrix}_k = \begin{Bmatrix} u_k - \bar{u} \\ v_k - \bar{v} \end{Bmatrix}, \quad (23)$$

where

$$\bar{u} = \frac{1}{4} \sum_{k=1}^4 \tilde{u}_k \cdot \hat{\mathbf{b}}_1, \quad \bar{v} = \frac{1}{4} \sum_{k=1}^4 \tilde{u}_k \cdot \hat{\mathbf{b}}_2. \quad (24)$$

The translated points  $x_0$  and  $u_0$  are then scaled so that the average distance from the origin is  $\sqrt{2}$ . The scaled values,  $\hat{x}_0$  and  $\hat{u}_0$ , which are now unitless, are then used in Eq. (18) to solve for  $m$ . The components of  $m$ , which compose the matrix  $M$ , map control points  $\hat{x}_0$  to  $\hat{u}_0$ . The inverse,  $M^{-1}$ , maps  $\hat{u}_0$  to  $\hat{x}_0$ . The original vectors  $x$  and  $u$  are recovered from  $\hat{x}_0$  and  $\hat{u}_0$  by reversing the scaling and translation operations.

## Four-Point Algorithm

We summarize the four-point algorithm as follows:



**Figure 3.** Single forensic photograph showing arcing skid marks in the left travel lane and shoulder.

1. Select four control points  $x_k$ , no three of which are collinear, in image plane  $\mathcal{A}$ .
2. Select the corresponding four control points  $u_k$ , no three of which are collinear, in image plane  $\mathcal{B}$ .
3. Translate and scale points  $x_k$  to obtain  $(\hat{x}_0)_k$  for points in  $\mathcal{A}$ .
4. Translate and scale points  $u_k$  to obtain  $(\hat{u}_0)_k$  for points in  $\mathcal{B}$ .
5. Form  $K_m = b$  from Eq. (18) using translated and scaled values  $(\hat{x}_0)_k$ ,  $(\hat{y}_0)_k$ ,  $(\hat{u}_0)_k$ , and  $(\hat{v}_0)_k$ , and solve for  $m$ .
6. Construct  $M$  from  $m$ , and  $M^{-1}$  from  $M$ .
7. Use  $M$  and  $M^{-1}$  to map between conditioned points  $\hat{x}_0$  and  $\hat{u}_0$  in image planes  $\mathcal{A}$  and  $\mathcal{B}$ .
8. Use scaling and translation to recover  $x$  and  $u$  from  $\hat{x}_0$  and  $\hat{u}_0$ , respectively.

## RESULTS

We illustrate the results of the four-point algorithm on two case studies and a laboratory study. The first example considers what we regard as a classic application of photographic rectification: A skid mark deposited on a roadway on the day of the accident, memorialized only in a photograph. The analyst's objective is to determine the geometry of the skid mark.

The second example, included in the [Appendix](#), illustrates the use of aerial photography, available from map applications provided by sources such as Microsoft or Google. The analyst may wish to layer an aerial image of the site under a plan view of the survey points. Often the aerial photograph is not orthonormal to the site. To create an orthonormal image, the photograph must be rectified to the survey space.

The final example, also included in the [Appendix](#), investigates the algorithm's error associated with calculating known coordinates in a controlled setting.

We implement the algorithm in MATLAB® [14], which allows for digital image processing and computation in a single, unified program.

## Case Study 1

Consider the forensic photograph shown in [Figure 3](#). From this single photograph, we will use the four-point algorithm to rectify the image to obtain the geometry of the skid, which is utilized in accident reconstruction analysis with conservation of energy principles to determine the amount of kinetic energy, and hence speed, dissipated during the skid.

Remarkably, this method requires neither external camera parameters (position and orientation) nor internal camera parameters (focal length, pixel geometry) be known for image rectification.

We begin by selecting four control points that were surveyed during the post-accident scene inspection, indicated by ‘ $\times$ ’ in [Figure 4](#). We refer to this image as  $\mathcal{B}$ , which has units of pixels. Let the four control points be  $u_k$ , with labels obtained from point numbers in the site survey. We magnify the  $(1500 \times 1000)$  pixel image, and select pixel locations within the image that correspond to the control points. We record these pixel points in [Table 1](#). We convert the color photograph to black and white, since color requires three values (red, green, blue) per pixel, whereas black and white requires only one (grayscale between 0 and 255). For a pixel value  $p$ , we obtain a single grayscale pixel value from the RGB pixel value using [13]:

$$p_{\text{gray}} = 0.2989 p_{\text{red}} + 0.5870 p_{\text{green}} + 0.1140 p_{\text{blue}}. \quad (25)$$

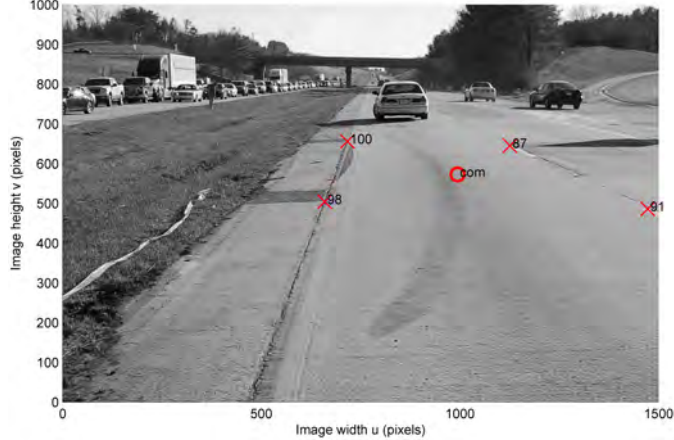


**Figure 4.** Forensic photograph with four control points  $(u)_k$  indicated by red ‘ $\times$ ’ and labels from the point numbers of the corresponding points in the survey. We refer to this image as  $\mathcal{B}$ , with units of pixels.

We next select the four corresponding control points, indicated by ‘+’ and numeric labels in [Figure 5](#). We refer to this image as  $\mathcal{A}$ , which has units of feet. Let the four control points be  $(x)_k$ .

**Table 1.** Image control points in  $\mathcal{A}$ , as surveyed, and the corresponding image control points in  $\mathcal{B}$ .

Point	Image $\mathcal{B}$		Image $\mathcal{A}$	
	$u$ (pixels)	$v$ (pixels)	$x$ (feet)	$y$ (feet)
100	717	656	129.5	-117.0
98	660	504	130.0	-168.0
91	1473	486	145.8	-175.2
87	1126	645	145.3	-131.3

**Table 2.** Consistency check of image control points in  $\mathcal{B}$ , mapped back to  $\mathcal{A}$  with  $M^{-1}$ .

Point	$M^{-1}$ (Image $\mathcal{B}$ )	
	$M^{-1}(u)$ (feet)	$M^{-1}(v)$ (feet)
100	129.5	-117.0
98	130.0	-168.0
91	145.8	-175.2
87	145.3	-131.3

We record these survey points in [Table 1](#). Other survey points are shown in [Figure 5](#), but not labeled with point numbers.

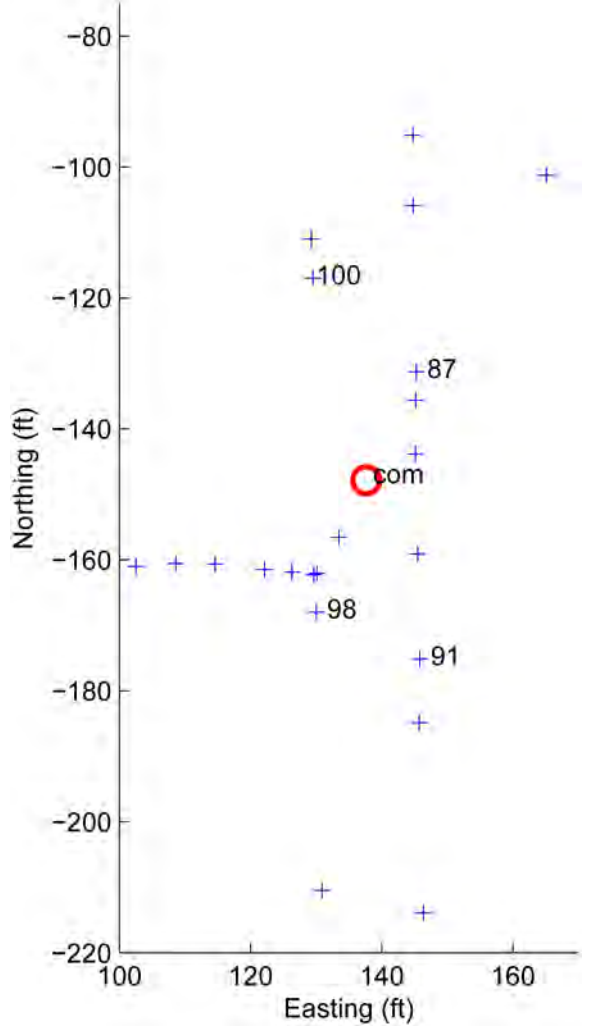


**Figure 5.** Subset of survey points, indicated by ‘+’, shown in the region of interest, with four control points  $(x)_k$  selected and labeled as survey points 100, 98, 91, and 87. We refer to this as image  $\mathcal{A}$ , with units of feet.

Following the four-point algorithm explicated here, we find the solution matrix  $K$  to have the following sub-blocks:

$$\begin{bmatrix} k_{11} & k_{12} \\ k_{21} & k_{22} \\ k_{31} & k_{32} \\ k_{41} & k_{42} \end{bmatrix} = \begin{bmatrix} -0.4598 & 1.7429 \\ -0.4309 & -1.1370 \\ 0.4611 & -1.5414 \\ 0.4295 & 0.9356 \end{bmatrix}, \quad (26)$$

and

$$\begin{bmatrix} k_{17} & k_{18} \\ k_{27} & k_{28} \\ k_{37} & k_{38} \\ k_{47} & k_{48} \\ k_{57} & k_{58} \\ k_{67} & k_{68} \\ k_{77} & k_{78} \\ k_{87} & k_{88} \end{bmatrix} = \begin{bmatrix} -0.5684 & 2.1546 \\ -0.6423 & -1.6949 \\ -0.9858 & 3.2952 \\ -0.2530 & -0.5512 \\ 0.1708 & -0.6475 \\ -0.1322 & -0.3489 \\ 0.1785 & -0.5968 \\ -0.1385 & -0.3017 \end{bmatrix}. \quad (27)$$

Referring back to Eq. (19), note that the  $k_{11}$  sub-block is repeated for the  $k_{54}$  sub-block. The  $K$  matrix has a condition number of 19.24, which is well-conditioned.

We find the mapping matrix  $M$  for this example to have the form

$$M = \begin{bmatrix} 2.6004 & -0.2147 & -0.1874 \\ 0.0909 & 0.2603 & 0.1162 \\ 0.0156 & 0.2459 & 1.0000 \end{bmatrix}. \quad (28)$$

Note the matrix, with a condition number of 11.56, is well-conditioned.



**Figure 6.** Survey points from survey space  $\mathcal{A}$  mapped forward to photographic space  $\mathcal{B}$ . Note control points for the pixel points and survey points overlap, and are labeled 100, 98, 91, and 87. The remaining survey points are plotted without labels. Yellow ‘x’ points mark the skid.

We then use matrix  $M$  to map the survey points from survey space  $\mathcal{A}$  to photographic (pixel) space  $\mathcal{B}$ . This mapping is depicted in Figure 6. The four control points selected in pixel space are indicated with a red ‘x’ and points from the survey space are shown by a blue ‘+.’ Large yellow ‘x’ points identify the skid.

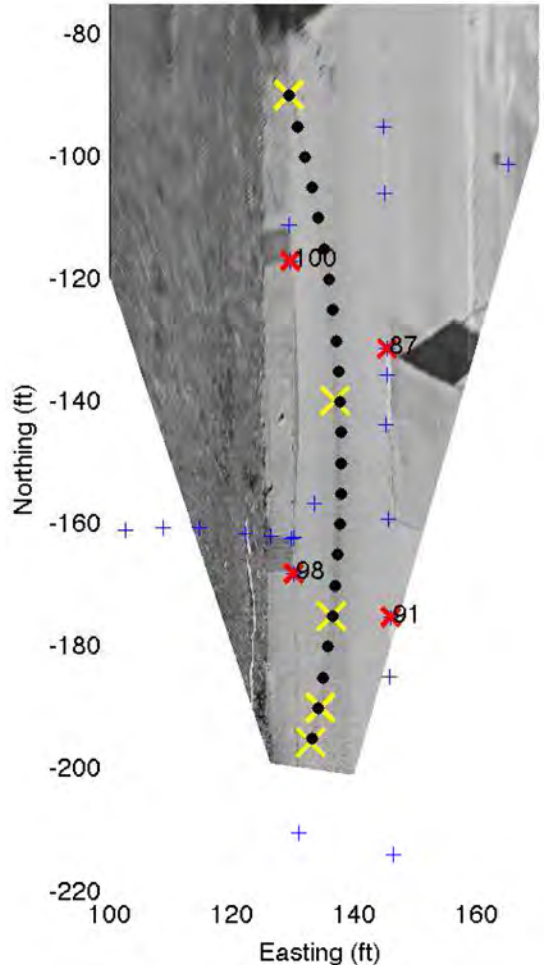


**Figure 7.** Photographic image  $\mathcal{B}$  mapped to survey space  $\mathcal{A}$ . Control points selected in  $\mathcal{B}$  are indicated by red ‘x’ and control points selected in  $\mathcal{A}$  are indicated by ‘+’ and numeric labels 100, 98, 91, and 87. Yellow ‘x’ points mark the skid.

The inverse map  $M^{-1}$  is applied to the pixel selections to check consistency of the map with the original selected control points in  $\mathcal{B}$  to their corresponding positions in  $\mathcal{A}$ , as shown in Table 2. Mapping the image in Figure 6 back into survey space using matrix  $M^{-1}$  results in the image shown in Figure 7.

The accuracy of the skid mark reconstructed using the presented four-point algorithm can be evaluated by comparing the image in Figure 7 to the image rectified by PhotoModeler [15] in Figure 8. The length of the skid mark

in [Figure 7](#) (107 feet), is within one percent of the length of the skid mark in [Figure 8](#) (106 feet), which is well within the accuracy acceptable for accident reconstruction purposes. In addition to the overall length, the four-point algorithm also produces good results with respect to the location of the skid mark on the roadway and the geometry (curvature) of the skid mark, as seen in [Figure 7](#).

## DISCUSSION

We have presented an algorithm that maps points between two image planes. The points appearing in the image planes are projections of points contained on a planar surface of an object.



**Figure 8. Photographic image  $\mathcal{B}$  rectified with the commercial software application PhotoModeler<sup>®</sup> [15].**

While there are numerous multipoint algorithms for image-to-image mapping, the four-point algorithm presented here is mathematically the simplest formulation that can be constructed for planar analysis. Many researchers have presented additional point and iterative algorithms as alternatives, citing numerical ill-conditioning as a disadvantage to the four-point algorithm [11].

If the control points picked from the images  $\mathcal{A}$  and  $\mathcal{B}$  are used without preconditioning, the resulting [Eq. \(19\)](#) indeed can suffer from conditioning problems. Observe from [Eq.](#)

[\(19\)](#) the direct dependence on  $x$  and  $u$  coordinates, which causes [Eq. \(19\)](#) to have multiple units within the matrix. There are units from  $\mathcal{A}$  (feet), units from  $\mathcal{B}$  (pixels), units from multiplication of  $\mathcal{A}$  with  $\mathcal{B}$  points (feet-pixel), as well as terms that have no units. While this hybridization of units within the matrix presents no mathematical problem, its presence immediately sparks the idea that perhaps some type of scaling would be helpful.

Consider further that the survey coordinates  $x$  are measured from an arbitrary reference datum. Not all surveyors pick  $(0, 0)$  as their datum. Indeed, many surveyors select offsets to their datum, e.g.,  $(1000, 1000)$ , from which all remaining survey points are registered. Immediately, we observe that surveys with larger distances, compared to those with smaller distances, will have worse conditioning when used directly in [Eq. \(19\)](#). This suggests that there might be a way to normalize the survey data regardless of measurement span, so that all surveys produce similar numerical behavior.

Similarly, consider the pixel span afforded by modern digital photography. In the first case example, the forensic photograph had a height of 1000 pixels and a width of 1500 pixels. Just as large distances engender ill-conditioning from the survey space  $\mathcal{A}$ , large pixel spans impart ill-conditioning from the pixel space  $\mathcal{B}$ .

Taking inspiration from Hartley [11], we translate and scale the selected control points prior to creating the correspondence map  $M$  in [Eq. \(7\)](#). This preconditioning results in stable and reliable matrices, well-suited to inversion. The condition numbers obtained for the examples presented here are well within a satisfactory range.

There are guidelines for the selection of control points. First, all control points must reside on a plane  $\partial\Omega$  of the body  $\Omega$  being imaged in  $\mathcal{A}$  and  $\mathcal{B}$ . Additionally, all control points must be visible in both  $\mathcal{A}$  and  $\mathcal{B}$ . In our examples, it typically is not a problem for the control points to be visible in  $\mathcal{A}$ , since the survey contains an orthographic plan view of all points. However, photographs used for  $\mathcal{B}$  rarely contain all points. Indeed, this restriction guides our process of first selecting a suitable photograph with four easily identifiable points, and subsequently identifying the corresponding control point data from the survey. Second, no three of the four control points may be collinear. This requirement is necessary to give full rank to matrix  $K$  in [Eq. \(19\)](#). Finally, if there is a specific region of interest (e.g., a skid mark) contained within the photograph, it is advantageous to select control points around the perimeter of the region, as demonstrated in our first case study.

The mapping of pixel space  $\mathcal{B}$  back to survey space  $\mathcal{A}$  is demonstrated by the map of the photograph shown in [Figure 6](#) back to [Figure 7](#). The foreground in image  $\mathcal{B}$ , taken of the

roadway from the perspective of a camera, appears condensed (narrower) in image  $\mathcal{A}$ , whereas the background in image  $\mathcal{B}$  appears expanded (wider) in  $\mathcal{A}$ . This result is to be expected. In the foreground, the transverse distance captured by the 1500 pixel width of the photograph is on the order of 15 feet, covering the left shoulder and part of the left travel lane. In contrast, in the background, the same 1500 pixel width of the photograph traverses a distance several times that of the foreground width. It therefore makes sense that rectification of image  $\mathcal{B}$  expands the pixels from foreground to background, as seen in [Figure 7](#).

Caution should be used when mapping *all* points in a survey from survey space  $\mathcal{A}$  to photographic space  $\mathcal{B}$ . Since the algorithm requires that all points of the body  $\Omega$  lie on a planar surface  $\partial\Omega$ , any survey points with an elevation above or below the points of interest in the survey space will get mapped forward to  $\mathcal{B}$  unreliably. This behavior can be observed in the top right corner of [Figure 6](#), where survey points with elevation above the roadway get mapped out of the roadway plane.

## **CONCLUSION**

We presented a simple yet robust algorithm for mapping points between image planes. The algorithm required that only four control points be identified in each image for successful mapping between the image pair. The algorithm was based on perspective geometry mathematics, which we outlined in our development of the algorithm.

The utility of the four-point method to the accident reconstruction community was demonstrated with two case studies and a laboratory study. The three examples showed that the algorithm is numerically well-conditioned and provided reliable results. Numerical inputs and outputs from each example were provided, allowing other analysts to use the four-point algorithm presented here, and check their implementation against known results.

## **REFERENCES**

1. Faugeras, O., "Three-Dimensional Computer Vision: A Geometric Viewpoint," The MIT Press, Cambridge Massachusetts, ISBN: 0-262-06158-9, 1993.
2. Ma, Y., Soatto, S., Kosecka, J., Sastry, S.S., "An Invitation to 3-D Vision, From Images to Geometric Models," Springer-Verlag, New York, ISBN: 0-387-00893-4, 2004.
3. Szeliski, R., "Computer Vision: Algorithms and Applications," Springer-Verlag, London, ISBN 978-1-84882-934-3, 2011, doi:[10.1007/978-1-84882-935-0](https://doi.org/10.1007/978-1-84882-935-0).
4. Quan, L., "Image-Based Modeling," Springer Science+Business Media, New York, ISBN: 978-1-4419-6678-0, 2010, doi:[10.1007/978-1-4419-6679-7](https://doi.org/10.1007/978-1-4419-6679-7).

5. Cliff, W., MacInnis, D., and Switzer, D., "An Evaluation of Rectified Bitmap 2D Photogrammetry with PC-Rect," SAE Technical Paper [970952](#), 1997, doi: [10.4271/970952](https://doi.org/10.4271/970952).
6. Fenton, S. and Kerr, R., "Accident Scene Diagramming Using New Photogrammetric Technique," SAE Technical Paper [970944](#), 1997, doi: [10.4271/970944](https://doi.org/10.4271/970944).
7. Pepe, M., Grayson, E., and McClary, A., "Digital Rectification of Reconstruction Photographs," SAE Technical Paper [961049](#), 1996, doi: [10.4271/961049](https://doi.org/10.4271/961049).
8. Toglia, A., Stephens, G.D., Michalski, D.J., Rodriguez, J.L., "Applications of PhotoModeler in Accident Reconstruction," Proceedings of IMECE2005, ASME International Mechanical Engineering Congress and Exposition, Nov 5-11, 2005.
9. Faugeras, O., "Stratification of Three-Dimensional Vision: Projective, Affine, and Metric Representations," *J Opt Soc Am A*, Vol 12, No 3, March 1995.
10. Longuet-Higgins, H.C., "A Computer Algorithm for Reconstructing a Scene from Two Projections," *Nature*, Vol 293, No 10, September 1981.
11. Hartley, R.I., "In Defense of the Eight-Point Algorithm," *IEEE Transactions on Pattern Analysis and Machine Intelligence*, Vol 19, No 6, June 1997.
12. Heckbert, P.S., "Fundamentals of Texture Mapping and Image Warping," Master's Thesis, UCB/CSD 89/516, Computer Science Department, University of California Berkeley, May 1989.
13. Ware, C., "Information Visualization, Perception for Design," Elsevier Morgan Kaufmann, San Francisco, ISBN: 1-55860-819-2, 2004.
14. MATLAB® version R2012b (8.0) Natick, Massachusetts: The MathWorks Inc., 2012.
15. PhotoModeler®, Photogrammetry software developed by Eos Systems Inc, 210-1847 West Broadway, Vancouver BC V6J 1Y6, Canada, 2012.

## **CONTACT INFORMATION**

Chad B. Hovey, Ph.D.  
Hovey Consulting LLC  
4801 Lang Avenue NE, Suite 110  
Albuquerque NM 87109  
Telephone: 505-345-2070  
[chad.hovey@hoveyconsulting.com](mailto:chad.hovey@hoveyconsulting.com)

## **ACKNOWLEDGEMENT**

We thank Ms. Emily S. Gu for her assistance with the measurement and photography of the laboratory scene.

## APPENDIX

### APPENDIX A

#### CASE STUDY 2

In this example, we follow the same methods developed in first study, but compress some of the details for the sake of brevity. As before, points selected in pixel space are indicated by ‘ $\times$ ’ and in survey space are indicated by ‘ $+$ .’

We select four control points, which are recorded in [Table 3](#), checked for consistency in [Table 4](#), and indicated by ‘ $\times$ ’ in [Figure 9](#).

*Table 3. Image control points in  $\mathcal{A}$ , as surveyed, and the corresponding image control points in  $\mathcal{B}$ .*

Point	Image $\mathcal{B}$		Image $\mathcal{A}$	
	$u$ (pixels)	$v$ (pixels)	$x$ (feet)	$y$ (feet)
159	933	463	928.7	478.3
154	283	367	822.2	456.8
121	410	194	843.4	414.4
117	964	275	933.9	432.6

From a survey of the scene, we have survey points as shown in [Figure 10](#).

*Table 4. Consistency check of image control points in  $\mathcal{B}$ , mapped back to  $\mathcal{A}$  with  $M^{-1}$ .*

Point	$M^{-1}(\text{Image } \mathcal{B})$	
	$M^{-1}(u)$ (feet)	$M^{-1}(v)$ (feet)
159	928.7	478.3
154	822.2	456.8
121	843.4	414.4
117	933.9	432.6

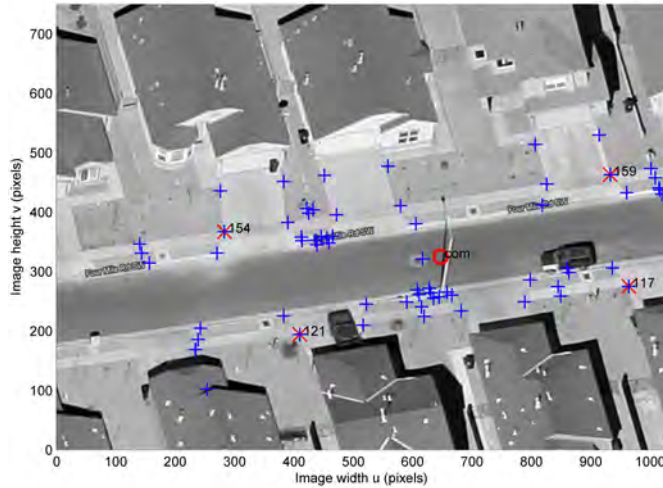


*Figure 9. Survey points from survey space  $\mathcal{A}$  mapped forward to photographic space  $\mathcal{B}$ . Note control points for the pixel points and survey points are coincident, and are labeled 159, 154, 121, and 117. The remaining survey points are plotted without labels.*

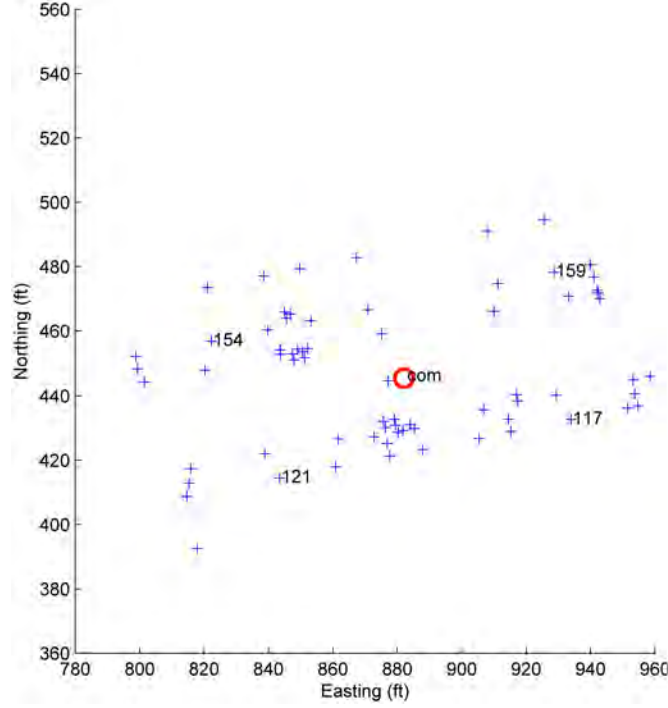


**Figure 10.** Survey points with four control points ( $x_k$ ) selected and labeled as survey points 159, 154, 121, and 117. We refer to this as image  $\mathcal{A}$ , with units of feet.

Following the four-point algorithm explicated here, we find the solution matrix  $K$  to have the following sub-blocks:

$$\begin{bmatrix} k_{11} & k_{12} \\ k_{21} & k_{22} \\ k_{31} & k_{32} \\ k_{41} & k_{42} \end{bmatrix} = \begin{bmatrix} 1.1937 & 0.8385 \\ -1.5324 & 0.2879 \\ -0.9895 & -0.7963 \\ 1.3282 & -0.3301 \end{bmatrix}, \quad (29)$$

and

$$\begin{bmatrix} k_{17} & k_{18} \\ k_{27} & k_{28} \\ k_{37} & k_{38} \\ k_{47} & k_{48} \\ k_{57} & k_{58} \\ k_{67} & k_{68} \\ k_{77} & k_{78} \\ k_{87} & k_{88} \end{bmatrix} = \begin{bmatrix} -1.5113 & -1.0616 \\ -2.4770 & 0.4654 \\ -1.0422 & -0.8387 \\ -1.8642 & 0.4634 \\ -0.7318 & -0.5141 \\ 0.2871 & -0.0539 \\ -0.5737 & -0.4617 \\ 0.2930 & -0.0728 \end{bmatrix}. \quad (30)$$

Note that the  $k_{11}$  sub-block is repeated for the  $k_{54}$  sub-block in Eq. (19). The  $K$  matrix has a condition number of 8.39, which is well-conditioned.

We find the mapping matrix  $M$  for this example to have the form

$$M = \begin{bmatrix} 1.0573 & 0.0064 & -0.0021 \\ 0.0117 & 0.7140 & 0.0001 \\ -0.0014 & 0.0014 & 1.0000 \end{bmatrix}. \quad (31)$$

The  $M$  matrix has a condition number of 1.48, which is well-conditioned. This matrix  $M$  is nearly equal to the identity matrix  $I$ , indicating the points imaged in  $\mathcal{A}$  are nearly the same as their expression in  $\mathcal{B}$ . Indeed, this concept can be seen by observing the aerial photography is nearly, but not fully, perpendicular to the subject roadway surface.

The rectified image is shown in [Figure 11](#). Note that items from the perspective aerial image, such as shadows, are preserved in the rectified image, since pixels maintain their color values, while their position values are stretched or compressed according to the mapping function  $M$ . We elected to crop the aerial image to include only the roadway and the northern driveways. These areas were the focus of the subject investigation. Also, the side views of the houses, present in the oblique aerial (see [Figure 9](#)), were potentially confusing when observed in the rectified view ([Figure 11](#)).

## LABORATORY DATA STUDY

In this example, we utilize floor tiles of known dimension as a reference study and examine the algorithm's error associated with estimating the known coordinates of the center of the scene. The floors tiles compose a black and white square checkered pattern. Each black and white square measures two feet in side length.

The reference photograph, shown in [Figure 12](#), was taken with a digital camera, intentionally oriented at a shallow elevation to the horizon. The shallower the camera angle is to the subject, the more sensitive the results will be to pixel selection. Conversely, the more perpendicular the camera angle is to the subject, the less sensitive the results will be to pixel selection.

Two perpendicular measuring tapes define a coordinate system in the planar floor and intersect at point 1 with defined coordinates (100, 100) feet.

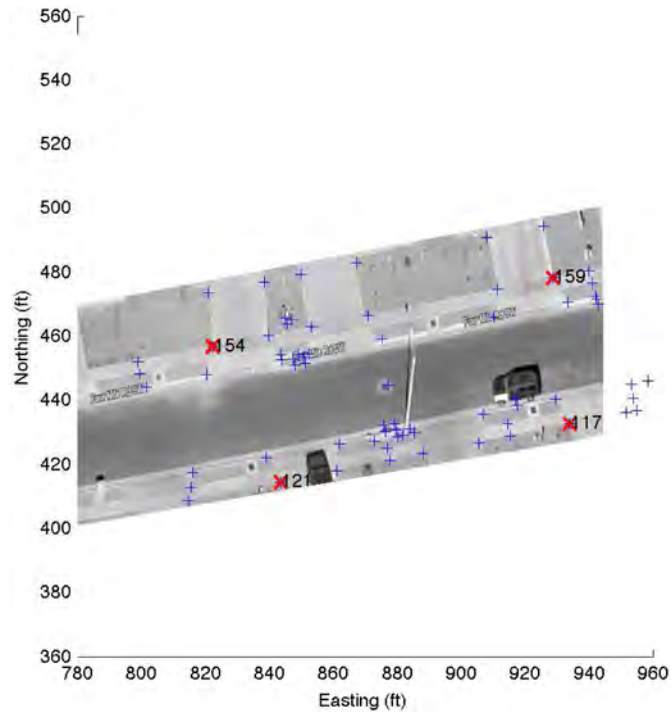


**Figure 11.** Photographic image  $\mathcal{B}$  mapped to survey space  $\mathcal{A}$ . Control points selected in  $\mathcal{B}$  are indicated by red 'x' and control points selected in  $\mathcal{A}$  are indicated by '+' and numeric labels 159, 154, 121, and 117.

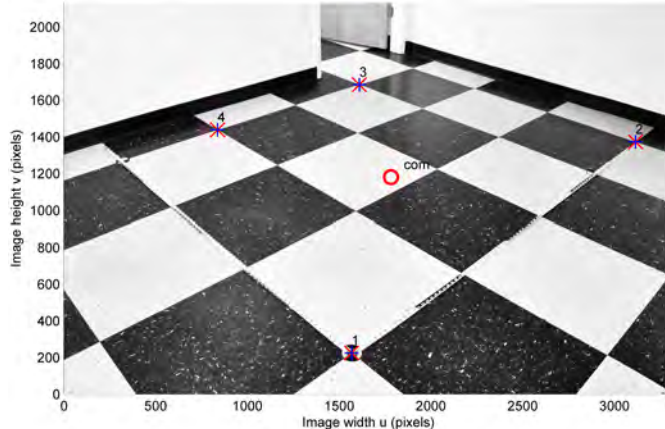


**Figure 12.** Reference photograph with grid of floor tiles of known dimension. Four control points  $(u)_k$  selected and labeled as survey point 1, 2, 3, and 4. We refer to this as image  $\mathcal{B}$ , with units of pixels.

We select four control points, which are recorded in [Table 5](#), checked for consistency in [Table 6](#), and indicated by ‘ $\times$ ’ in [Figure 12](#).

Following our four-point algorithm, we find the solution matrix  $K$  to have the following sub-blocks:

$$\begin{bmatrix} k_{11} & k_{12} \\ k_{21} & k_{22} \\ k_{31} & k_{32} \\ k_{41} & k_{42} \end{bmatrix} = \begin{bmatrix} -1.3147 & -0.9860 \\ 1.3147 & -0.9860 \\ 0.6573 & 0.9860 \\ -0.6573 & 0.9860 \end{bmatrix}, \quad (32)$$

and

$$\begin{bmatrix} k_{17} & k_{18} \\ k_{27} & k_{28} \\ k_{37} & k_{38} \\ k_{47} & k_{48} \\ k_{57} & k_{58} \\ k_{67} & k_{68} \\ k_{77} & k_{78} \\ k_{87} & k_{88} \end{bmatrix} = \begin{bmatrix} -0.4165 & -0.3124 \\ -2.5822 & 1.9366 \\ 0.1676 & 0.2513 \\ -0.9153 & 1.3729 \\ -1.8509 & -1.3882 \\ -0.3729 & 0.2797 \\ -0.4886 & -0.7330 \\ 0.2504 & -0.3756 \end{bmatrix}. \quad (33)$$

**Table 5.** Image control points in  $\mathcal{A}$ , as surveyed, and the corresponding image control points in  $\mathcal{B}$ .

Point	Image $\mathcal{B}$		Image $\mathcal{A}$	
	$u$ (pixels)	$v$ (pixels)	$x$ (feet)	$y$ (feet)
1	1568	224	100	100
2	3116	1372	108	100
3	1610	1684	106	106
4	838	1438	102	106

**Table 6. Consistency check of image control points in  $\mathcal{B}$ , mapped back to  $\mathcal{A}$  with  $M^{-1}$ .**

Point	$M^{-1}(\text{Image } \mathcal{B})$	
	$M^{-1}(u)$ (feet)	$M^{-1}(v)$ (feet)
1	100	100
2	108	100
3	106	106
4	102	106

Note that the  $k_{11}$  sub-block is repeated for the  $k_{54}$  sub-block in Eq. (19). The  $K$  matrix has a condition number of 5.47, which is well-conditioned.

We find the mapping matrix  $M$  for this example to have the form

$$M = \begin{bmatrix} 0.8661 & -0.9400 & 0.0271 \\ 0.4272 & 0.4778 & 0.2116 \\ 0.1834 & 0.1781 & 1.0000 \end{bmatrix}. \quad (34)$$

The  $M$  matrix has a condition number of 2.45, which is well-conditioned. The rectified image is shown in Figure 13.

To examine the algorithm's error, we sample the center of a white square, outlined with a solid blue line to indicate the known (surveyed) dimensions and a dashed red line to indicate the rectified dimensions. The center of the white square is located at (103, 103) feet, as shown in Figure 13 and magnified in Figure 14.

The center of the white square estimated from the rectified image is located at (103.0231, 103.0125) feet. The distance between the actual and predicted centers is 0.0263 feet (0.3152 inches). Since our unit of measure is feet, the error for the point sampled is 0.0263 feet/feet = 2.63%.

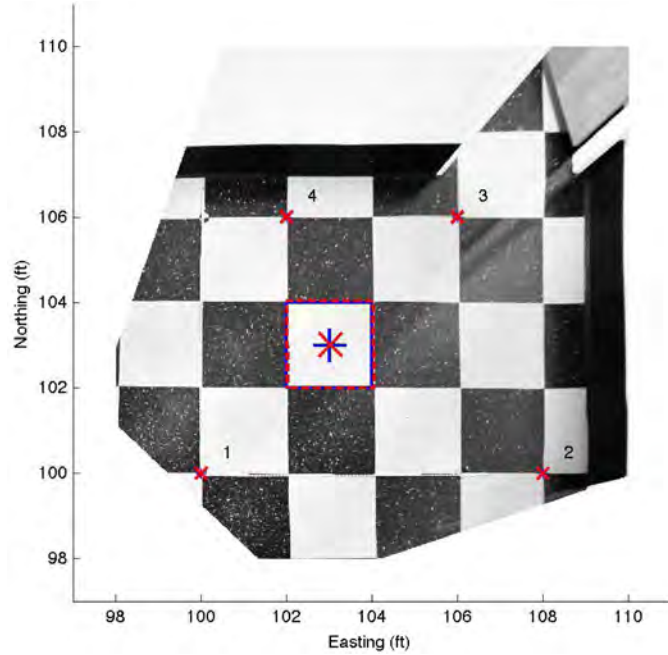


**Figure 13. Photographic image  $\mathcal{B}$  mapped to survey space  $\mathcal{A}$ . Control points selected in  $\mathcal{B}$  are indicated by red 'x' and control points selected in  $\mathcal{A}$  are indicated by '+' and numeric labels 1, 2, 3, and 4.**

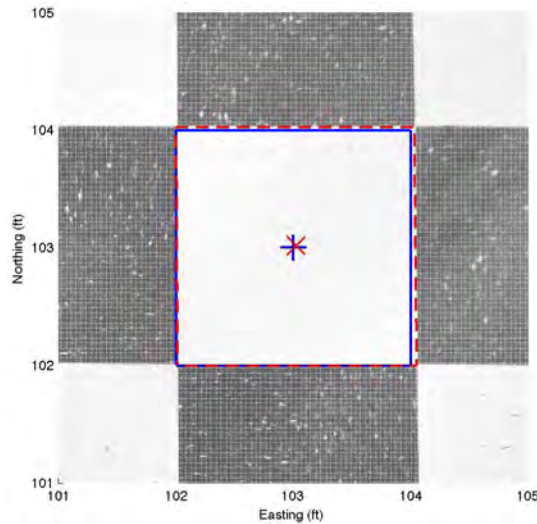


**Figure 14. Magnification of subject white square from Figure 13. The known center of the white square is shown with a blue '+' at (103, 103) feet. The estimated center from rectification is shown with a red 'x'.**

The Engineering Meetings Board has approved this paper for publication. It has successfully completed SAE's peer review process under the supervision of the session organizer. This process requires a minimum of three (3) reviews by industry experts.

All rights reserved. No part of this publication may be reproduced, stored in a retrieval system, or transmitted, in any form or by any means, electronic, mechanical, photocopying, recording, or otherwise, without the prior written permission of SAE.

ISSN 0148-7191

Positions and opinions advanced in this paper are those of the author(s) and not necessarily those of SAE. The author is solely responsible for the content of the paper.

**SAE Customer Service:**

Tel: 877-606-7323 (inside USA and Canada)

Tel: 724-776-4970 (outside USA)

Fax: 724-776-0790

Email: [CustomerService@sae.org](mailto:CustomerService@sae.org)

**SAE Web Address:** <http://www.sae.org>

**Printed in USA**